



Numerical analysis of isolated end-flattened steel bars under compression in space trusses

Henrique de Araujo Rosa Cruz, Luciano M. Bezerra, Welington Vital da Silva, Ramon Silva
University of Brasilia, Brazil
henrique.arcrúz@gmail.com, lmbz@unb.br, welington.vital@gmail.com, ramon.silva@unb.br

ABSTRACT. This research aims to characterize the behavior of isolated end-flattened steel bars under compressive loading, in which global instabilities or excessive local deformations represent a significant part of the causes of structural collapse. The association of numerical analyses using the finite element method (FEM) with previously collected experimental data is performed, and their respective results are the core object of critical analysis in this work. Numerical simulations are based on the modified Riks method, complemented in part by modal analysis, whose results demonstrate the occurrence of the aforementioned failure modes in prototypes with slenderness ratios varying in the spectrum from 20 to 200. Finally, the analytical formulations that describe the phenomenon from the approach of global and local instabilities incorporated into current normative expressions are applied in a comparison with the results gathered in the numerical approach.

KEYWORDS. End-flattened steel bars, Three-dimensional trusses, Global and local instabilities, Steel structures.



Citation: Cruz, H. A. R., Bezerra, L. M., Silva, W. V., Silva, R., Numerical analysis of isolated end-flattened steel bars under compression in space trusses, *Frattura ed Integrità Strutturale*, 63 (2023) 271-288.

Received: 28.08.2022

Accepted: 04.12.2022

Online first: 10.12.2022

Published: 01.01.2023

Copyright: © 2023 This is an open access article under the terms of the CC-BY 4.0, which permits unrestricted use, distribution, and reproduction in any medium, provided the original author and source are credited.

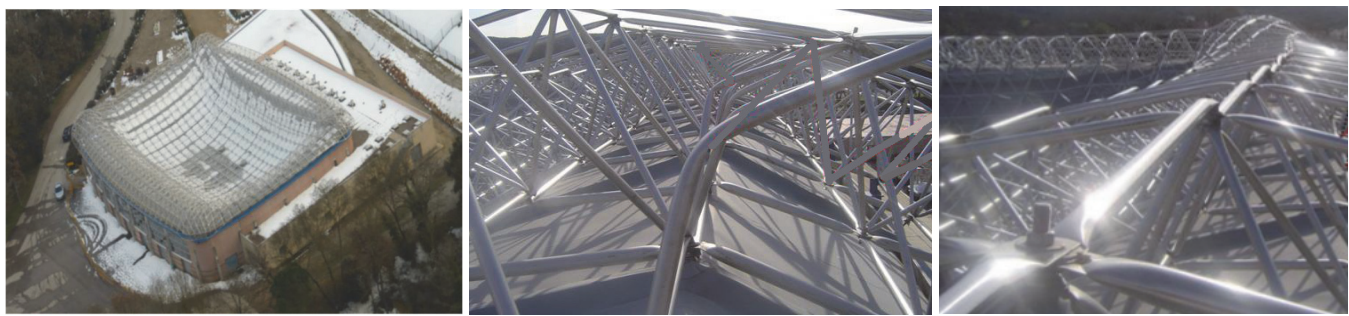
INTRODUCTION

The application of three-dimensional trusses as a structural system solution for different types of engineering work is notorious. This fact is due to a set of factors, such as its inherent resilience and its efficiency in the transmission of acting loads, which, in general, allow the design of slender and economically advantageous structures. Spatial trusses are often adopted as roof supports for sports gymnasiums, airports, industrial warehouses, and train stations – civil works usually designed to overcome large spans and maintain the structure's own weight value at an optimal level. A space truss type that has been frequently adopted as a structural system worldwide is the one composed of hollow circular cross-section bars, whose ends are previously flattened to promote coupling with other connection members by use of a single bolt. According to Bezerra et al. and Silva et al. [1-2], the simplicity and low cost of its construction method are relevant factors in its choice among engineering professionals. Despite this fact, some of its critical features, such as potential bending moments generated by eccentricity in the connections and the reduced rigidity due to the flattening process, must be duly considered in the designing process Silva et al [3]. It is imperative to establish specific normative criteria that provide an efficient and safe application of this type of structural element Freitas et al. [4-5]. Fig. 1 shows an example of these truss

members. It presents details of the connection system described above and illustrates the failures of some diagonal truss elements due to the characteristics aforementioned, with record of the first space truss collapse in Brazil in 1994.



Figure 1: Connection configuration of the end-flattened steel bars (a) and the collapse of a three-dimensional truss (b) [1].



(a)



(b)



(c)

Figure 2: Types of failure of space trusses with bars under compression. (a) Failures in space trusses with flattened-ends of the bars. (b) Fault in the roof space truss of the Dutch football club FC Twente. (c) Failure at the end of the space truss bars with cross section variation in the Shah Alam Stadium football in Malaysia.

Failure due to instability of bars subjected to compression has resulted in progressive collapse of several lattice roofing systems around the world, as presented in the technical literature [6-16]. Some recent examples of global collapse of structural systems composed of bars subjected to compression are briefly presented. In 2010, a roof of a sports gymnasium located in Spain, in space truss with flattened bars, collapsed due to snow loading, which resulted in buckling of the diagonals of the trusses [17]. The following year, in 2011, the Dutch football club FC Twente made an extension to their football stadium, with the execution of a space lattice roof, which during assembly resulted in the roof collapse, with bars buckling Karel Terwel et al [18-19]. Already in 2013, another failure of a coverage in space truss using bar with reduced section in conical shape occurred in the Shah Alam Stadium football at Malaysia. The report carried out by the Malaysia technical team concluded that the collapse was due to buckling of the bars and in conjunction with the rupture of several connections [2,20-21]. In this context, the Fig. 2 shows the different types of global collapse in bars under compression. Therefore, reliably predicting the strength of the bar under compression is very important to structural designers. However, the design codes do not present formulations for reducing the section of flattened-ends bars.

In the research carried out by Dundu [22] on the strength and stability characteristics of space trusses made up of steel bars with flattened extremities, the author describes two forms of failure for the main structural elements, when subjected to compressive loads: global buckling or excessive deformation of the transition zone of cross-sections at the ends of the bars. There is a significant correlation between the form of failure that a specific element presents and its respective slenderness. Furthermore, it was shown that the diameter-to-thickness ratio also influences the manifestation of one of the phenomena to the detriment of the other. The conclusions obtained from the study were that bars with high slenderness and low diameter-to-thickness ratios tend to fail due to global buckling by bending; bars that had a low slenderness and high diameter-to-thickness ratios generally failed due to excessive deformation in the transition zones of their ends. The impact that the number of holes for the bolts in the connections of the bars exerts on their compressive strengths was also investigated in the referenced work. However, no measurable changes in the load capacity have been detected by varying such feature. The configuration of the testing of the isolated bars with stamped ends and the different failure modes noticed in the experimental tests are shown in Fig. 3.

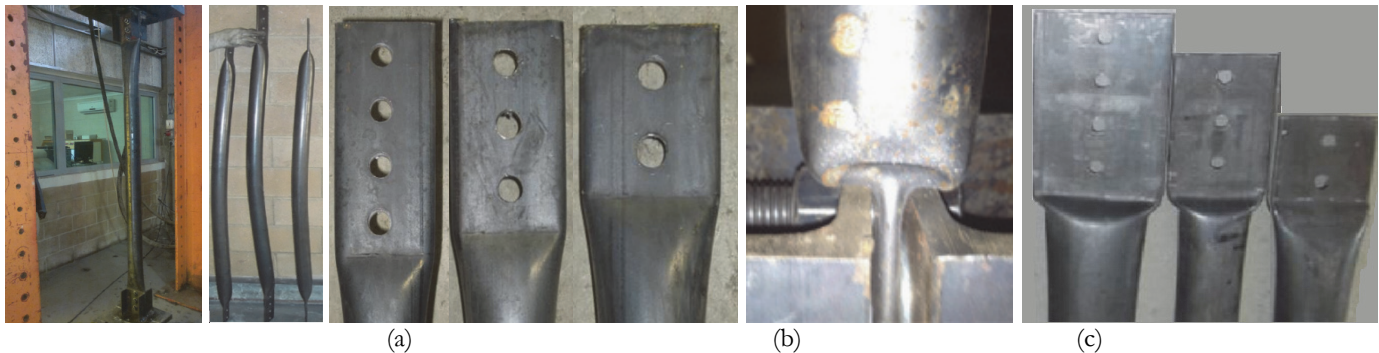


Figure 3: Failure modes of insulated bars with stamped ends: (a) experimental set. (b) global buckling. (c) and excessive deformation of the transition zone of cross-sections [22].

In the research by Silva [23], extensive studies were conducted on the structural behavior of three-dimensional trusses, especially on alternatives to connecting systems, as they represent a critical region regarding the origins of failures and collapses of engineering works. In the cited research, the history of structural systems for space trusses developed worldwide is summarized. Their inherent characteristics are presented, in addition to the proposition of new patented systems. For the experimental program, emphasis was given to the structural system of three-dimensional trusses comprised of end-flattened steel bars and single bolt connections. The tests to determine the mechanical properties of the steel used in the experiments and the tests of isolated bars are treated in this paper as direct subsidiary sources of information for its development.

Aiming to extend the understanding of the phenomenon of instability of three-dimensional trusses composed of end-flattened steel bars, this work proposes the systemic numerical analysis of these structural elements submitted separately to compressive loading. In a first phase, nine finite element prototypes of these bars are developed, whose geometric and mechanical properties are based on the specimens tested by Silva [23]. Such simulations cover a spectrum of slenderness ratios ranging from 20 to 100. This parameter has been chosen for the categorization of the prototypes given its predictive influence on the phenomenon under study. In addition, other six prototypes with slenderness ratios in the range of 100 to 200 were built. Compound simulations were then carried out based on the combination of modal analysis with analysis by the modified Riks method. All the simulations described above were conducted by use of the commercial software Abaqus® [24-25]. With these results, a qualitative comparison was made between the structural behavior of the numerical specimens

and the general code specifications for the predicted compressive strength of prismatic steel bars. The concepts of maximum load of compressive strength, maximum displacements, and deformations were explored in the simulations, as well as the stress fields developed in the structures during the application of the loads.

The paper structure is divided as follows: at first, the introduction presents a research about space trusses' mechanical behavior and history of collapses, based on papers regarding especially trusses composed by end-flattened steel bars. In the sequence, the experimental program made by Silva [23] is described, where the geometry and material properties of its prototypes serves as the basic initial input data for the numerical analysis to be developed. The next section is dedicated to the description of the numerical modelling of the end-flattened steel bars under compressive loads, shows step by step the constitution of the finite element models, passing through the applying of the boundary conditions and loads, the partition of the prototypes, the meshing generation process and the general settings to perform the simulations. The results obtained from the numerical analysis is then evaluated and compared with code formulations' results. Finally, it is emphasized that the contribution of this paper consists of nonlinear numerical simulation with Von Mises criterion, using a unit load step with Riks algorithm of the ABAQUS library, with automatic increment size. In which different lengths of tubes were simulated with flattening at the ends with slenderness between 20 and 200 submitted centered compression without eccentricity. This is because in the design standards the loss of resistance of the bars with flattening at the ends are not considered and several accidents have been recorded over the years.

EXPERIMENTAL PROGRAM

The carbon steel used in the experiments, according to the nomenclature established by the American Iron and Steel Institute (AISI) and the Society of Automotive Engineers (SAE), is called AISI 1020. The good formability and weldability of this type of steel encourage its frequent specification by designers. It is a material of usual application in the construction of three-dimensional trusses for spans of up to 30 m [23].

Tensile tests were carried out with the aid of the universal machine model EMIC DL-30000, which has a load capacity of 300 kN. A total of nine specimens from the lot supplied were analyzed at an extension rate of 0.010 mm/min, in which samples were taken from the ends and central regions of the bars. Fig. 3 exemplifies the execution of this experiment.

The results obtained from the experiments for the mechanical properties of the material are consistent with the manufacturer's specifications, in which the elastic modulus is close to 200 GPa, the yield strength was determined at 198 MPa and the ultimate strength was equal to 248 MPa. In addition, the measured elongation at break, based on a measurement of 50 mm, was 30% strain (mm/mm), and the associated Poisson ratio was 0.29.

The effective lengths of the tested bars were determined in the following based on the slenderness ratios addressed in the research of Silva [23], which vary on a scale between 20 and 100. The upper limit of the slenderness index was thus established due to the geometric limitations of the testing machine's frame. The total length of the bars was therefore maintained in the range of 490 mm to 1565 mm. The thickness of the thin-walled bars is equal to 0.95 mm. Fig. 4 provides details on the tested specimens.

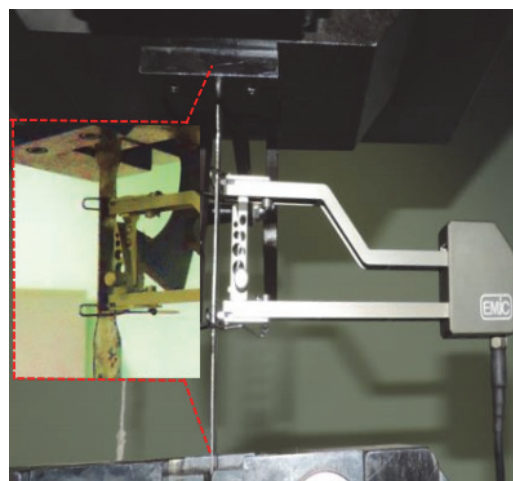


Figure 3: Tensile test at room temperature of sample of AISI 1020 steel [23].

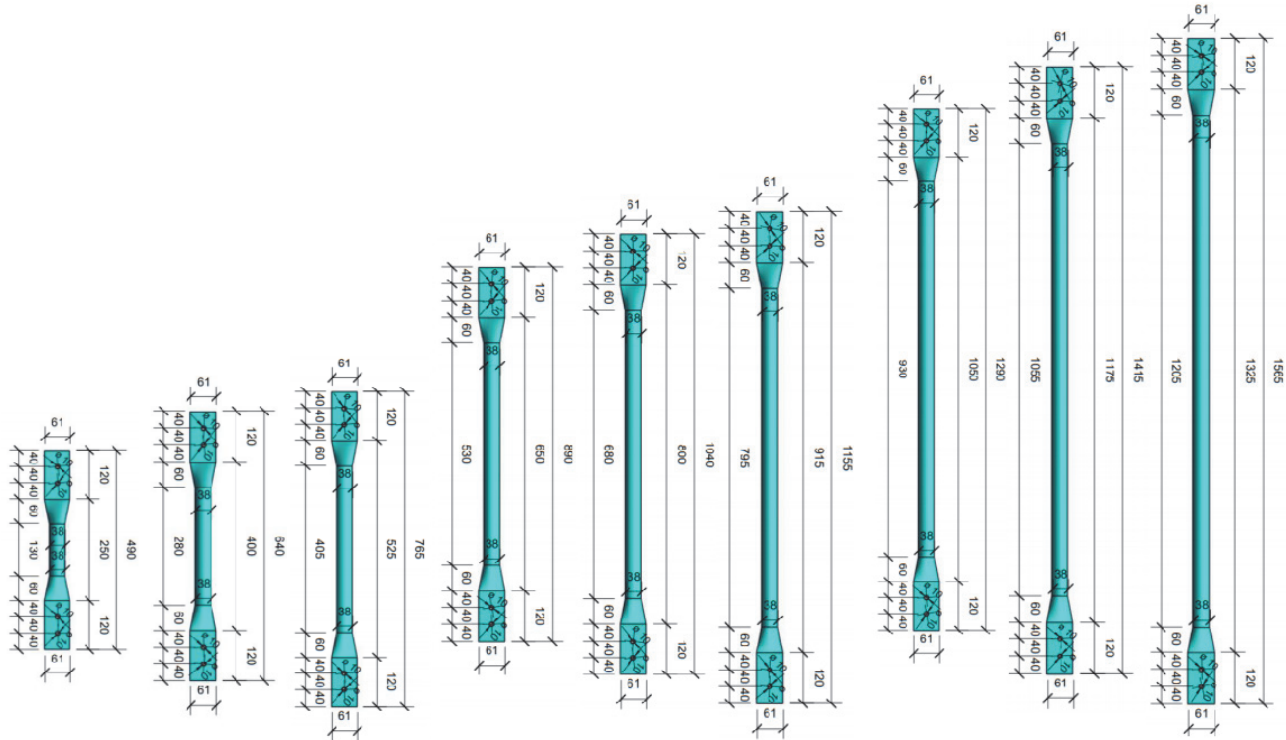


Figure 4: Geometric details of the tested bars [23].

To define the plastic behavior of the material in the numerical modeling process, it should be noted that the software Abaqus® establishes that the stress and strain input data must be informed in their true form and in ascending order. Thus, based on a representative set of tensile test data, made available directly by the author of the experiments in tables of ordered pairs of engineering stress and strain, its insertion into the program was performed after the proper conversion of the data into true stresses and strains. This procedure was executed with the successive application of Eqns. 1 to 3 in a spreadsheet program. The results obtained by converting the original data into true stresses and plastic strains are shown in Fig. 5.

$$\sigma = \sigma_{\text{eng}} (1 + \epsilon_{\text{eng}}) \quad (1)$$

$$\epsilon = \ln(1 + \epsilon_{\text{eng}}) \quad (2)$$

$$\epsilon_{\text{pl}} = \epsilon - \epsilon_{\text{el}} = \epsilon - \frac{\sigma}{E} \quad (3)$$

where:

σ is the true stress;

ϵ is the true strain;

σ_{eng} is the engineering stress;

ϵ_{eng} is the engineering strain;

ϵ_{pl} is the plastic deformation;

ϵ_{el} is the elastic deformation;

E is the elastic modulus of the material.

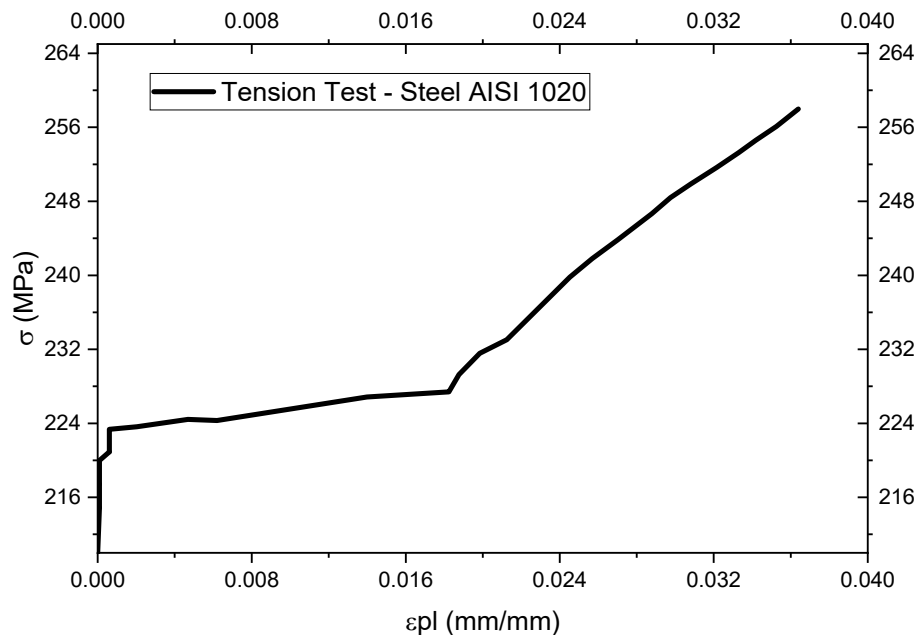


Figure 5: True stress data vs. plastic deformation of AISI 1020 steel.

ANALYTICAL STRENGTH OF BARS UNDER COMPRESSION

Euler's theory of bars is used to estimate the critical buckling load of column, since the stress in the column remains elastic. The critical buckling load is the maximum load that a column can withstand when it is on the verge of buckling. The buckling failure occurs when the length of the column is greater when compared with its cross-section [8]. The Euler's theory is based on certain assumptions related to the point of axial load application, column material, cross-section, stress limits, and column failure by compression. The validity of Euler's theory is subjected to a condition, that failure occurs due to buckling [15].

This theory does not consider the effect of direct stress in column, the out of plumb and residual stress, that is always present in column, and possible displacements of axial load application point from the center of the cross-section of the compressed bar, with emergence of eccentricities. As a result, the theory may overestimate the critical buckling load and normative corrections are carried out. Therefore, this section presents a comparison of the test results with existing design codes from of ABNT NBR 16239:2013 [26]; ANSI/AISC 360-16 [27]; Eurocode 3 Part 1.4 [28], and Canadian standard CSA-S16 [29]. With the FE modelling, comparison has been made according to test type of the compression of the bars. The analytical calculation of the bars under compression was considered with both ends pinned. All partial safety factors have been set to unitary to enable a direct comparison of the results.

The Brazilian standard of circular hollow sections ABNT NBR 16239:2013 [26] presents prescriptions for the determination of the axial compression strength of calculation for prismatic bars. It is emphasized that the standard provides resistance capacity without regarding the bars flattened-ends and eccentricities [30]. ABNT NBR 16239:2013 [26] considers that the sizing of bars under compression load must be carried out in accordance with the requirements of ABNT NBR 8800:2008 [31]. However, it presents its own curve to calculate the reduction factor associated with the axial compression load for tubular profiles [30]. Thus, the computation of the axial compression strength of calculation given by:

$$N_{c,Rd} = \frac{\chi Q A_g f_y}{\gamma_{a1}} \tag{4}$$

where, χ is the reduction factor associated with the compression strength; Q is the total reduction factor associated with local buckling χ Annex F of the standard; A_g is the gross cross-section area of the bar; f_y is the steel yield strength; γ_{a1} is the resistance factor equal to 1.1. The reduced slenderness ratio, λ_0 , is given by



$$\lambda_0 = \sqrt{\frac{QA_g f_y}{N_e}} \quad (5)$$

The elastic buckling axial force, N_e , is obtained by the expression:

$$N_e = \frac{\pi^2 EI}{(KL)^2} \quad (6)$$

On the other hand, the reduction factor associated to the compression strength, χ , is provided by NBR 16239:2013 [26] through the expression:

$$\chi = \frac{1}{(1 + \lambda_0^{4.48})^{1/2.24}} \quad (7)$$

In ANSI/AISC 360-16 [27] when dealing with elastic columns, the buckling stress is multiplied by a reduction factor of 0.877 over the elastic curve, to explain the effects of initial curvature according to Eqn. E3-3. Therefore, it is easy to obtain the ANSI/AISC 360-16 [27] equation in the elastic regime for columns with the Euler curve correction factor as follows in the Eqn. 8. If the column exhibits inelastic behavior, the flexural buckling stress based on the AISC E3-2 equation shown from Eqn. 9, which will be equal to 0.658 raised to the power of the reduced slenderness index, and multiplied by the yield strength of the steel.

$$\chi = \frac{f_{cr}}{f_y} = (0.658^{\lambda^2}) \quad \lambda\sqrt{Q} \leq 1.50 \quad (8)$$

$$\chi = \frac{f_{cr}}{f_y} = \left(\frac{0.877}{\lambda^2}\right) \quad \lambda\sqrt{Q} \geq 1.50 \quad (9)$$

$$\lambda = \frac{KL}{r} \sqrt{\frac{f_y}{\pi^2 E}} = \sqrt{\frac{QA f_y}{N_e}} \quad (10)$$

Therefore, what determines whether a column falls in the elastic or inelastic range depends on a single inequality given by the reduced slenderness index λ , whereas the design resisting force for bar with axial force is given by the Eqn. 11.

$$N_{e,Rd} = \frac{\chi Q A f_y}{\gamma_{a1}} \quad \text{with } \gamma_{a1} = 1.0 \quad (11)$$

At the design resistant axial force indicated in Eqn. 11, Q represents the reduction coefficient due to local buckling and $A f_y$ is the plastic strength of the cross-section. The compressive strength reduction factor χ , given to the buckling effect, as a function of the reduced slenderness of the compressed bar. Where N_e is the critical elastic buckling force of the bar, e , is applicable to the full range of rolled and welded profiles and tubes under centric compression.

The Eurocode 3 Part 1.4 [28] formulations for the determination of flexural buckling resistance are determined from Eqn. 12.



$$N_{c,Rd} = \frac{\chi A_{eff} f_y}{\gamma_{M1}} \quad \text{for class 4 cross-sections} \quad \gamma_{a1} = 1.0 \quad (12)$$

where A_{eff} is the effective area of Class 4 cross-sections, χ is the reduction factor accounting for buckling determined from Eqn. 13, and γ_{M1} is a partial safety factor and set equal to unitary for this comparison.

$$\chi = \frac{1}{\Phi + \sqrt{\Phi^2 - \lambda^2}} \quad \text{but } \chi \leq 1.0 \quad (13)$$

where the intermediate factor Φ and the non-dimensional member slenderness λ are defined by Eqn. 14 and Eqn. 15, respectively.

$$\Phi = 0.5 \left[1 + \alpha (\bar{\lambda} - \bar{\lambda}_0) + \bar{\lambda}^2 \right] \quad (14)$$

$$\bar{\lambda} = \sqrt{\frac{A_{eff} f_y}{N_{cr}}} \quad \text{for class 4 cross-sections} \quad (15)$$

In which α is an imperfection factor (taken as 0.49 for the sections investigated herein), λ_0 is the limiting slenderness taken as 0.4, and N_{cr} is the elastic critical buckling force for the relevant buckling mode based on the gross properties of the cross-section [32]. The strength of the bar under axial compression according to the requirements of code CSA-S16 [29] is based on a fully fixed column and with an initial imperfection of $L / 1000$ according to the 1P curve of the Social Science Research Council [33]. Unlike other international standards, the Canadian standard does not use a normalized relief curve, the equation for defining the axial compressive strength is simpler and more compact. In which, the resistance of a bar in compression, critical “Cr”, with buckling about any axis is defined as Eqn. 16 given by.

$$Cr = \phi A f_y (1 + \lambda^{2n})^{-1/n} \quad \text{with } n = 1.34 \quad (16)$$

$$\lambda = \frac{KL}{r} \sqrt{\frac{f_y}{\pi^2 E}} \quad (17)$$

NUMERICAL ANALYSIS

From the geometric characteristics of the end-flattened steel bars tested by Silva [23], as indicated in Fig. 4, the design of the base geometries of the numerical models concerning the first phase of simulations was made in the software AutoCAD®. Fig. 6 presents the details and denomination of the different regions of the bars. The bars’ geometries were exported individually in SAT (Standard ACIS Text) format files for the constitution of the numerical models. To perform the numerical analysis of the prototypes investigated in this research, the Finite Element Method (FEM) was applied by means of the computational tools provided by the software Abaqus®. After verifying the consistency of the dimensions of the models, the modeling of the mechanical properties of the steel used in the research proceeded as discussed previously. Since the prototypes are essentially composed of thin plates, whose thickness is equal to 0.95 mm, a shell-type cross-section was adopted as its representative shape.

By default, the program has a pre-defined initial phase, in which the system's starting boundary conditions are included. The extremities of the end-flattened steel bars were totally restrained in terms of displacements and rotations, except for the one associated with the acting compressive load, whose translational degree of freedom parallel to the longitudinal axis of the prototypes was released. To define the technique and analysis parameters, a new subsequential phase was created, where the modified Riks static general procedure was applied in order to capture any local unstable collapse of the models

and to consider the geometric and physical nonlinearities inherent to the phenomena under study. As the load is treated as an additional variable to the simulation, this method makes use of the arc length as the base quantity to measure the progress of the solution. Since one of the main goals of this work is to determine the maximum magnitude of the compressive load before the loss of stiffness and collapse of each specimen, the initial load value must be set below that limit. Based on the experimental results presented by Silva [23], which indicate ultimate resistance loads of a few units or tens of kilonewtons (kN) for the different slenderness levels of the bars, the initial load value was adopted as equal to 1.0 kN.

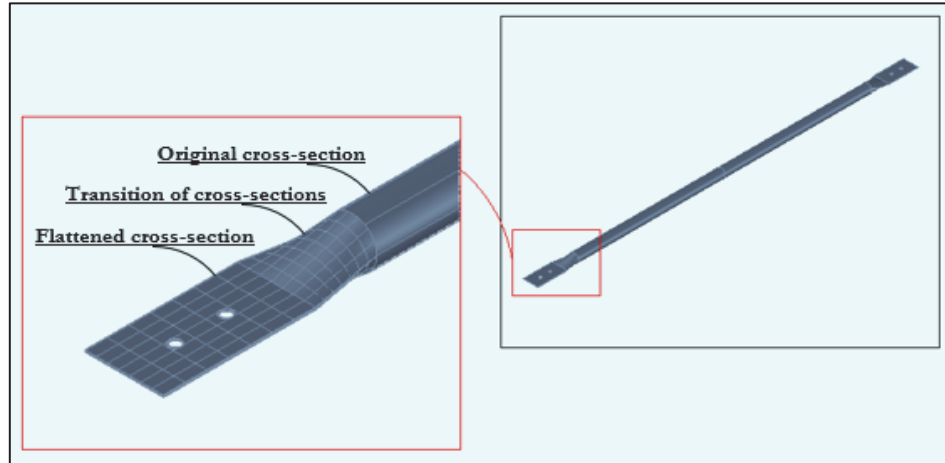


Figure 6: Details of the base geometry of the numerical models developed: regions of original cross-section, transition of cross-sections and flattened cross-section.

The development of the finite element meshes in Abaqus® originated from partitions previously made in the geometry of the prototypes, where domain subdivisions were prescribed along their edges to control the size of the elements generated in each specific region. For the general geometry of the models, an upper size restriction of 5 mm was imposed on the elements, while maximum dimensions of 2 mm were assigned to the geometry of the holes of the bolted connections. According to the description of the initial modeling stages, the bars are represented by numerical models with shell-type cross-sections, and therefore must contain finite elements of the same class. Among the finite element library of the software, the S4R type was chosen for the execution of the simulations. This is a four-node shell element type suitable for thin-walled structures, which makes use of reduced integration and hourglass control incorporated in its formulation. The geometry partitioning process mentioned above also allowed the application of the structured mesh generation technique to the numerical models. The mesh transition minimization algorithm was added to this procedure, aiming to guarantee the shape regularity of the finite elements and, thus, the accuracy of the results. Fig. 7 and Fig. 8 presents the finite element mesh pattern generated in this phase of the study.

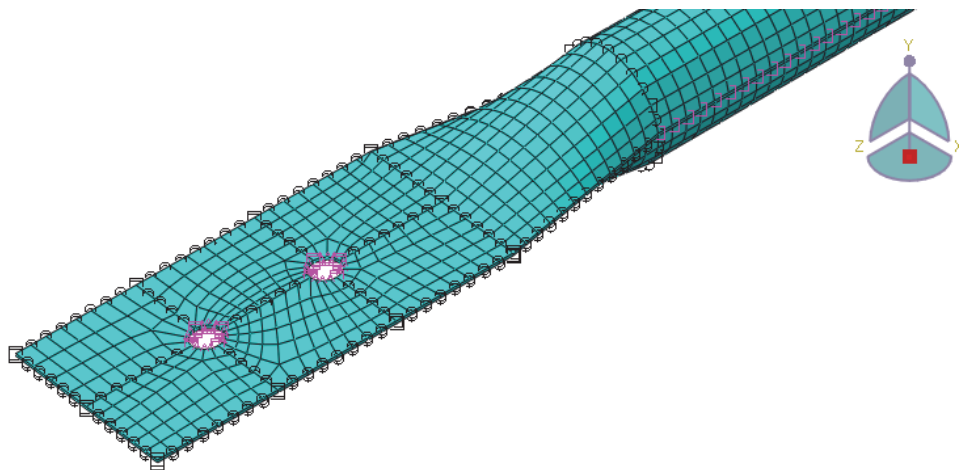


Figure 7: Finite element mesh pattern of the numerical models of the end-flattened steel bars.

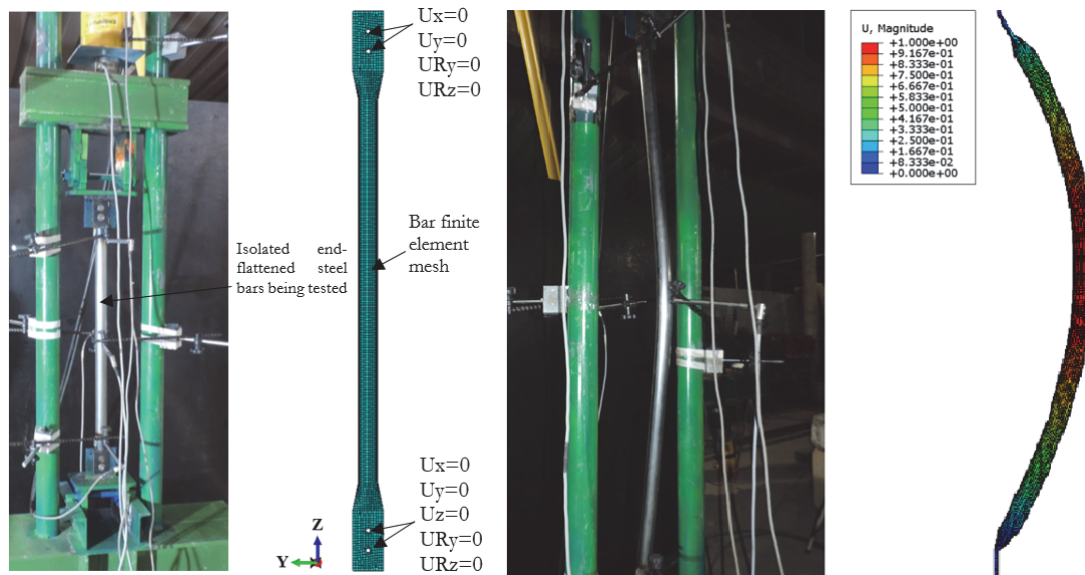


Figure 8: Boundary conditions of the numerical simulation of the bar under centered compression.

The numerical simulations were performed with increasing compressive loads on the models and concluded a few steps after reaching the ultimate strength load relative to each reference slenderness ratio of the bars. To this end, the equilibrium trajectories of the prototypes were monitored based on the increment data of the analysis and its Load Proportionality Factor (LPF). This quantity represents the value by which the load initially applied to the models must be multiplied to determine the load acting on the structure at a given stage or increment. Once the total load of 1.0 kN was established at the beginning of the simulations, the LPF directly indicates the load applied to the models, in kilonewtons. When obtaining negative increments for the LPF, the passage through the first critical point of the equilibrium trajectory of the specimens is thus configured. The results regarding the simulations of the end-flattened steel bars with slenderness ratios (λ) ranging from 20 to 100 will be presented and discussed along with the results obtained in the second phase of the numerical analysis in the proper section.

The numerical modeling of the end-flattened steel bars with slenderness ratios (λ) in the spectrum from 100 to 200 followed the methodology described for the previous modeling phase, regarding the execution of the geometry of the bars and the insertion of the properties of the AISI 1020 steel in the software, as well as the application of the boundary conditions, loading and definition of the finite element meshes. However, due to the susceptibility of these slenderer models to the global buckling failure mode, this complementary set of numerical analyses required the implementation of adjustments in its approach. In order to certify that the models developed previously do not show a tendency to the referred failure mode, the model with a slenderness ratio equal to 100, the slenderest of the first group, was also included in this new series of simulations.

The geometric configuration of the other specimens evaluated in this work, whose slenderness ratios range from 100 to 200, was modeled at a later stage by the continuous extension of the lengths of the first set of bars. All the flattened and transition regions of cross-sections remained with their original characteristics.

Due to the symmetry of the studied prototypes in terms of geometry, boundary conditions and compressive axial loading, the eventual manifestation of global buckling in the numerical analyses by the single application of the modified Riks method is prevented. Thus, the models needed an additional mechanism so that this failure mode could be captured in the simulations. The way chosen in this work to overcome the presented problem is based on the introduction of initial imperfections in the numerical models, which were established as a limit value of 1% of the bars' wall thickness, in millimeters, to preserve the concept of the experiment idealized. The type of analysis previously conducted was replaced by a numerical composite analysis, resulting from the sequential association of a modal buckling analysis with an analysis by the modified Riks method.

By performing the modal analysis of the bars with a straight initial geometry and slenderness ratios (λ) in the range of 100 to 200, the deformed configuration of each prototype is obtained and their first and main buckling mode is determined. For the eigenvalues to directly represent the generating load of the global buckling of the bars, the total initial load was kept unitary. The translation of these buckling modes into nodal displacements was effectively recorded in the output files of the Abaqus® software, which are visually available to the user of the program with the aid of its post-processing tools. Fig. 9



shows the deformed configuration of an example of a prototype after the buckling analysis, in which its displacements were increased with a scale factor of $1e+02$ for better visualization of the phenomenon in question. After recording the displacements of the meshes' nodes in the program's result files, such information is incorporated into the initial conditions of the geometry of the further analysis by the Riks method, which is structured as explained in the first phase of the numerical analyses.

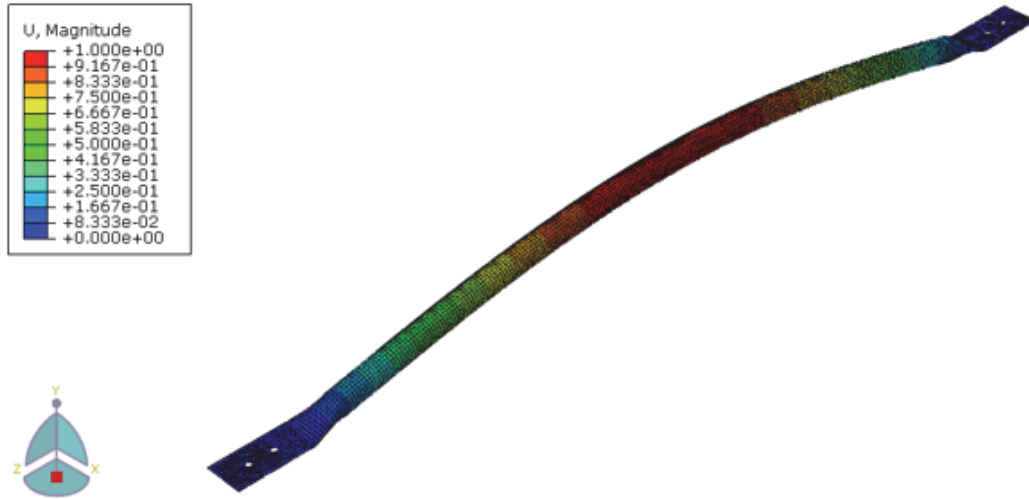


Figure 9: Example of the main buckling mode of a numerical model in Abaqus® software. Unit of displacements in millimeters (mm).

RESULTS AND DISCUSSION

From the analysis of the results collected, the first noticeable fact is the equivalence between the first and second phases of simulations of the prototype with a slenderness ratio equal to 100. In terms of the structural failure mode presented by the specimens, namely the excessive deformation and collapse of their extremities, as well as the magnitude of the ultimate compressive load, the models were consistent. In this sense, the second phase of simulations had the role of ratifying the results obtained in the previous phase. These results are summarized in Figs. 10 and 11.

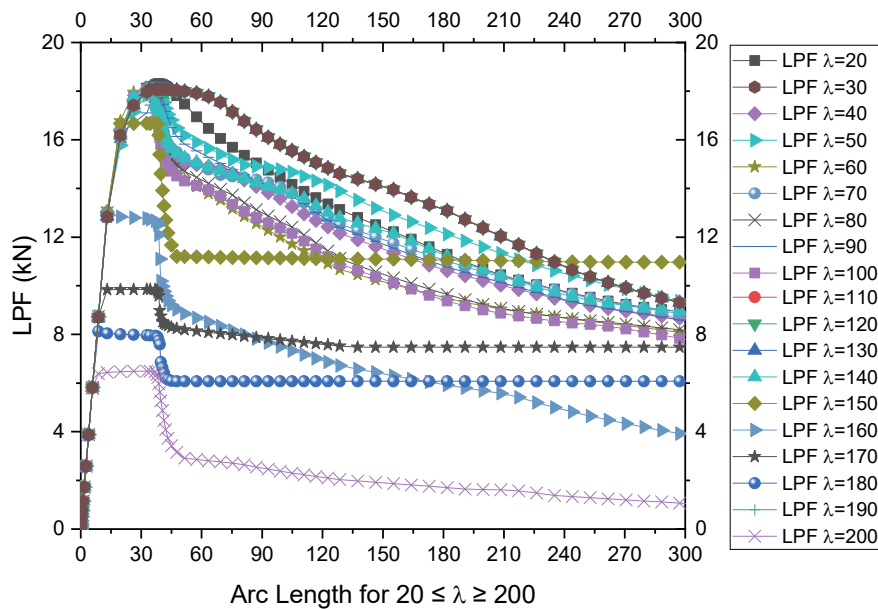


Figure 10: LPF data vs. Arc length of the end-flattened steel bars' numerical simulations – $20 \leq \lambda \leq 200$.

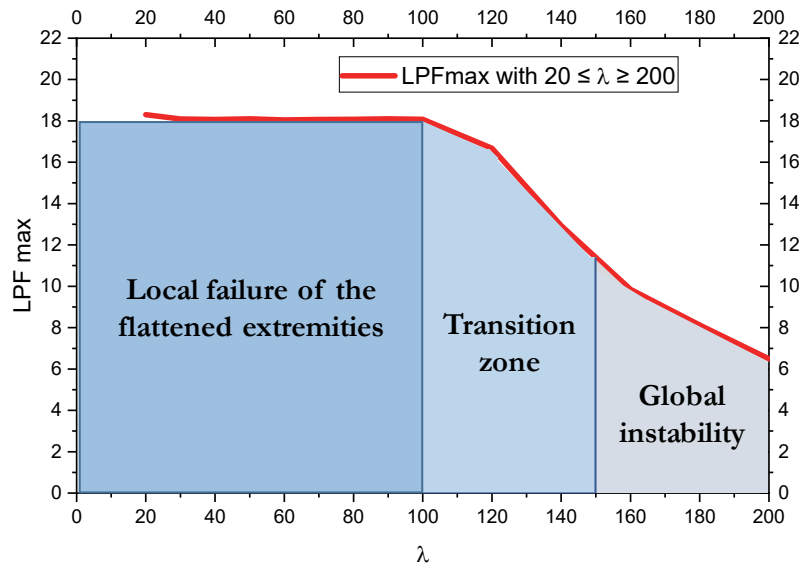


Figure 11: Max LPF data. vs. Slenderness ratio (λ) of the end-flattened steel bars' numerical simulations – $20 \leq \lambda \leq 200$.

Based on the collected data, it is observed that the value of ultimate resistance load of the numerical models with slenderness ratios (λ) ranging from 20 to 100, represented by the maximum LPFs, did not present a significant correlation with the slenderness of the bars, where its value was approximately constant at 18.0 kN. This fact is corroborated by the failure mode exhibited by the prototypes, in which the local failure of the transition zone of cross-sections at their ends was present in all the models developed. The experimental tests conducted by Silva [23] presented coincident results regarding the structural failure form of the end-flattened steel bars for this slenderness range. With the monitoring of the LPF during each numerical simulation, the formation of the first plasticizing point in these regions is accurately observed when the LPF's increment value becomes negative - that is, when the loss of rigidity of the system begins. Fig. 12 exemplifies the simulation step previously described. For the stress analysis carried out in this study, the von Mises equivalent stress criterion was adopted as a reference, given its wide applicability in the steel structures' field [3,5,34-36].

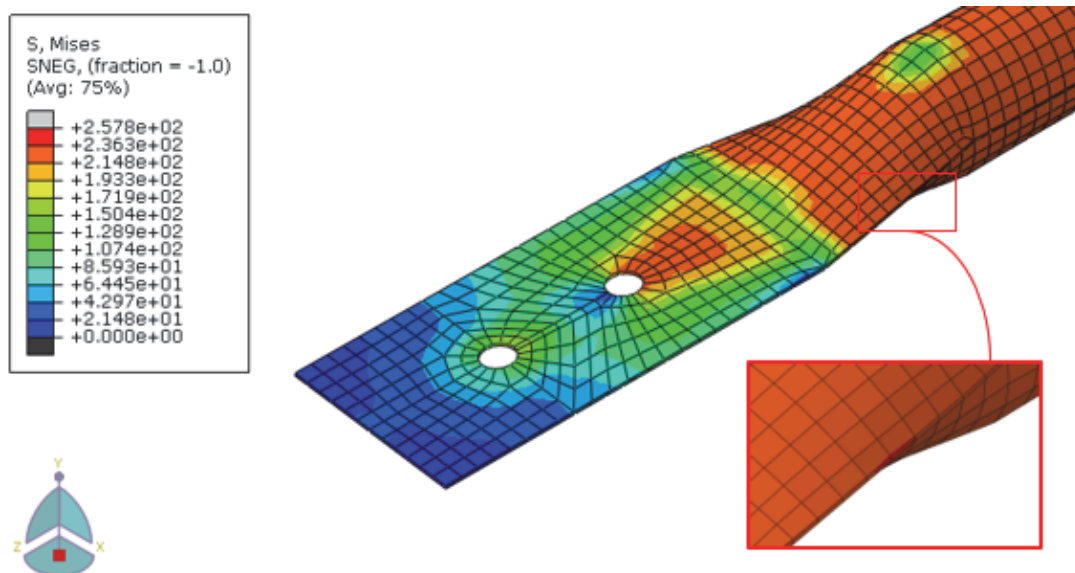


Figure 12: Simulation step in the Abaqus® software with the beginning of the plasticizing of the transition zone of cross sections at the flattened ends of the numerical models. Unit of von Mises stresses in MegaPascal (MPa).

Due to the ideal conditions pertinent to the numerical modeling process, it appears that the results obtained represent an upper limit of critical load when designing bars with stamped ends. The inclusion in the analysis of semi-rigid supports, geometric imperfections or initial loading eccentricities, residual stresses or deformations, for example, has the potential to



reduce the ultimate resistance load of the structural elements in question. The fact that the critical loads of the shorter bars present little variability due to the local rupture mode of the totality of the specimens indicates that such values basically translate into the resistance of the transition zone of cross sections of these bars. Thus, by modifying the geometric patterns of the bars, especially the extension of the transition zone of cross-sections, as well as the diameter-to-thickness ratio of the original circular cross-section, a corresponding change in the value of the ultimate load resisted by the specimens is expected, even if keeping the slenderness ratios in the reference range of 20 to 100. Further experimental and numerical investigations should be carried out in a parametrical study to put these considerations into test and are recommended as a future line of research. Finally, an aspect of potential impact on the structural efficiency of the bars in terms of their geometric properties, especially in the transition zone of cross-sections, is the development of the stress fields during the compressive loading. The evaluation of the distribution of von Mises stresses in the numerical models was carried out in the successive steps of analysis, so that an absolute uniformity was observed between the collected data of the set of smaller slenderness ratios. Fig. 13 shows the loading stages in terms of percentage of the ultimate resistance load (P_{ult}) and the stress fields of a representative numerical simulation, based on the specimen of slenderness ratio equal to 100.

From the analysis of these results, at first it is possible to observe the stress concentration at the spot of application of the compressive loading in the prototypes, with its intensity being comparatively higher in the innermost hole in relation to the outer one. As the cross-sections of the flattened region after the holes are analyzed, towards the center of the bars, the spreading and homogenization of the stresses are perceived, as foreseen by the Saint-Venant principle. When the transition zone of cross-sections is reached, the stress distribution becomes more complex due to the variable geometry of its cross-sections, in which a higher stress concentration is noted on the sides of the models with the conjugate stress relief in the upper and lower regions. Viewing the models in plan, as shown in Fig. 4, the load eccentricity existing between the lateral ends of the flattened regions and the original circular cross-section region is evidenced, which corroborates the fact that there is a greater stress on the sides of the prototypes to the detriment of complementary upper sub-regions. When evaluating the original circular cross-section region of the models, a new uniformity of the stresses is evident when examining cross-sections closer to the geometric center of the bars.

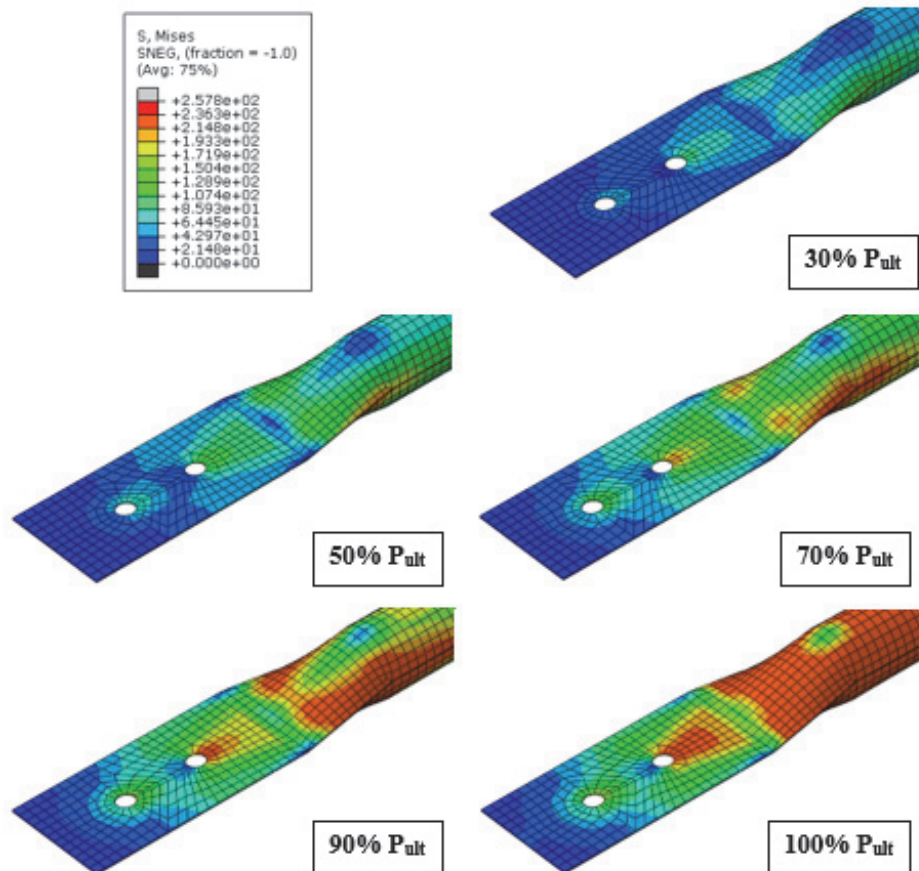


Figure 13: Development of the stress fields in the numerical models in Abaqus® software. Unit of von Mises stresses in MegaPascal (MPa).

As the results of the other models are evaluated, in ascending order of slenderness ratio, there is a gradual reduction in the ultimate resistance load of the prototypes. A common factor in this set of simulations is the failure mode of the specimens, in which global buckling prevailed over local instabilities. Figs. 14 through 15 illustrate the collapse of one of the numerically tested models, with slenderness ratio equal to 200, in the analysis increment referring to its ultimate resistance load and, thus, to the beginning of its global instability. Fig. 16 shows the local failure due to the flattening of the bar, for small indices of slenderness ($20 \leq \lambda \leq 100$). To provide greater clarity to the visualization of the specimen deformation at this loading stage, a scaling factor of $5e+01$ was applied to the displacements of the finite element mesh.



Figure 14: Displacements referring to the global buckling of a numerical model example in Abaqus® software, in millimeters (mm).

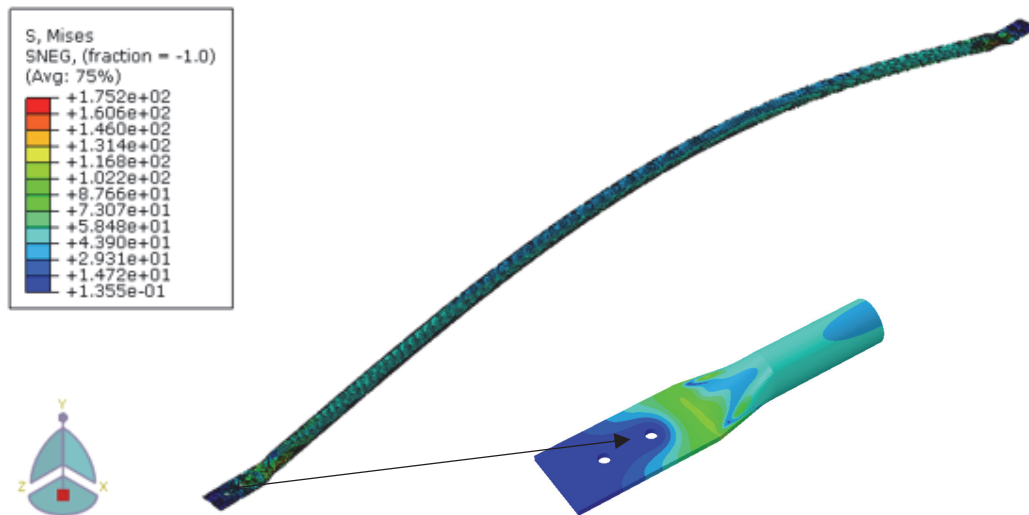


Figure 15: Von Mises stresses referring to the global buckling of a numerical model example in Abaqus® software, in MegaPascal (MPa).

The displacement and stress results of specimens with slenderness ratios contained in the range of 120 to 200 indicate a brief transition between failure modes due to excessive local deformation of the flattened ends and global buckling of the prototypes. In such a transition, a partial plasticizing is observed in the transition zones of cross-sections of the model with a slenderness ratio equal to 120, although global instability is its characteristic collapse mode. In the following numerical analyses, related to the three models of slenderness immediately greater, a reduction in the level and a change in the location of the highest tensions can be observed. In this set of analyses, the critical stresses of the prototypes moved from the flattened ends of the bars to their central regions. To conclude the series of simulations, the structural behavior of the model with a slenderness ratio equal to 200 under compressive load was defined by the global buckling of the prototype still in the linear elastic regime. This fact is attested by the von Mises stress level reached at this stage of the analysis, whose values are entirely below the yield strength of AISI 1020 steel.

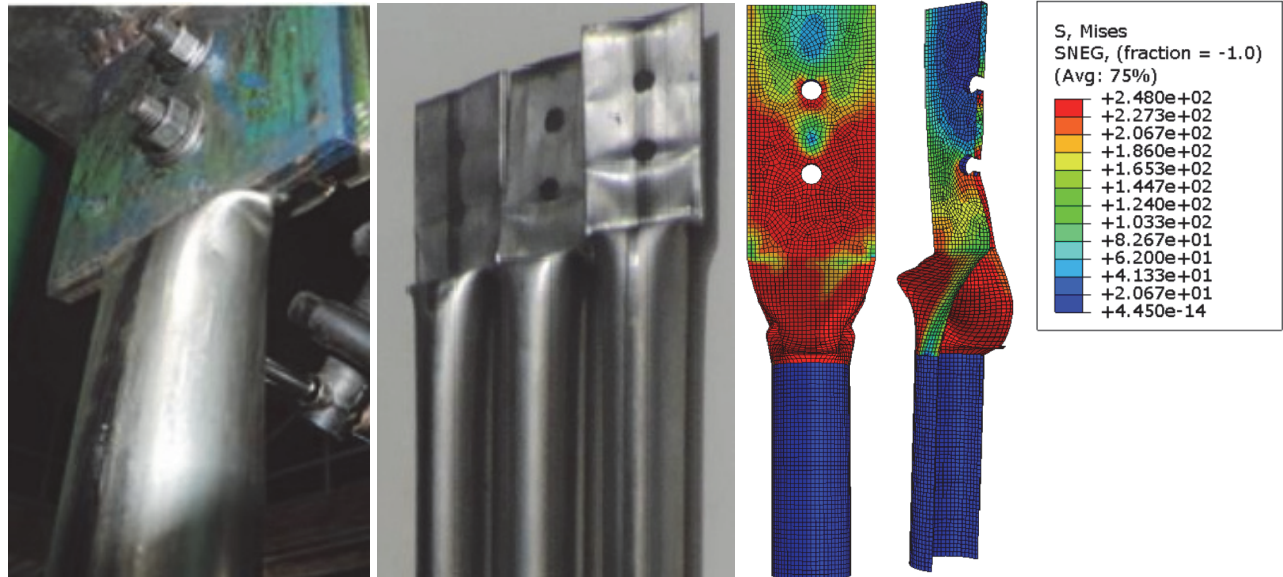


Figure 16: Von Mises stresses at the extremities of a numerical model example in Abaqus® software, in MegaPascal (MPa).

The ultimate limit state design methodology of linear compressed elements referring, for example, to the Brazilian code NBR 16239:2013 [26] and ABNT NBR 8800:2008 [31], encompasses the local and global effects of instability of such structures for a variety of configurations of cross-section geometric shapes. However, in the case of bars with flattened ends, the normative provisions do not indicate a specific approach to determine the influence of the stamping process and the consequent geometry on the structural strength of the designed element. To verify the form of the ultimate load vs. slenderness ratio curves relative to the numerical simulations and the normative values, Fig. 17 contains the plotting of both data sets. The curve regarding the resistance capacity of the profiles foreseen by the design criteria of the aforementioned code, namely P_{ult} – Normative criteria, is shown in Fig. 16 in terms of characteristic values. This choice was made by aiming to compare the numerical and analytical results under the same criterion of variability in the mechanical properties of the steel, since, in the numerical simulations, the component material of the modeled bars is deterministically constituted. Consequently, this procedure allows a more isolated assessment of the effect of stamping on the axial compressive strength of hollow cross-sections.

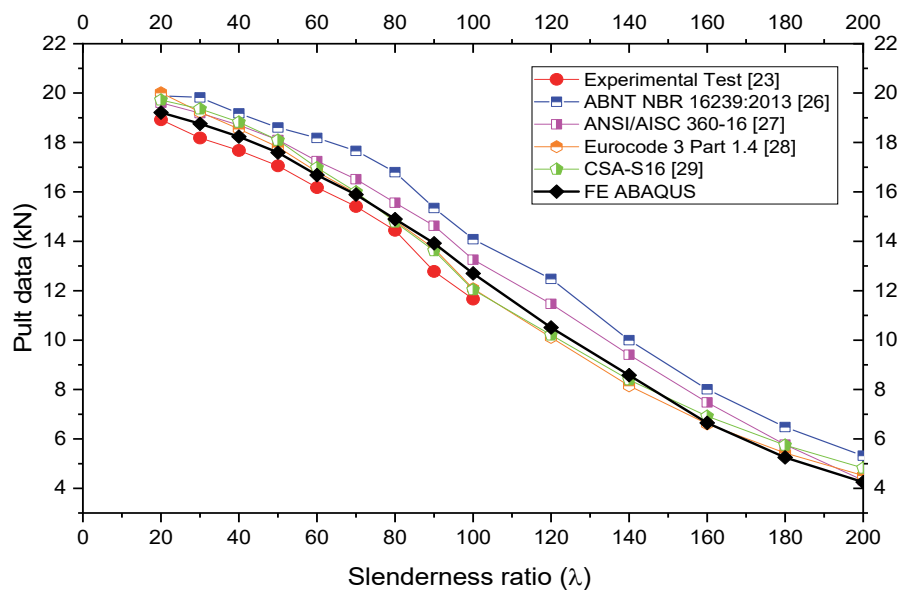


Figure 17: P_{ult} data vs. Slenderness ratio (λ) of the numerical simulations of the end-flattened steel bars and the application of the design criteria of the ABNT NBR 8800:2008 [31] code.



The experimental, analytical and numerical results are presented in Tab. 1.

D _{ext.} (mm)	D _{int.} (mm)	D/t	r (mm)	L _{ef} (mm)	λ (L _{ef} /r)	A _g (mm ²)	*N _{exp} (kN)	N _{NBR} ¹ (kN)	N _{AISC} ² (kN)	N _{EC-3} ³ (kN)	N _{CSA-16} ⁴ (kN)	NUMERICAL ABAQUS (kN)
38	36.1	40	13.1	250	20	110.57	18.62	19.88	19.61	20.01	19.72	19.20
38	36.1	40	13.1	400	30	110.57	18.18	18.85	19.19	19.23	19.36	18.75
38	36.1	40	13.1	525	40	110.57	17.67	18.78	18.70	18.55	18.82	18.23
38	36.1	40	13.1	650	50	110.57	17.05	18.60	18.10	17.81	18.09	17.59
38	36.1	40	13.1	800	60	110.57	16.16	18.18	17.25	16.81	16.98	16.68
38	36.1	40	13.1	915	70	110.57	15.40	17.66	16.51	15.95	16	15.89
38	36.1	40	13.1	1050	80	110.57	14.44	16.79	15.56	14.83	14.78	14.89
38	36.1	40	13.1	1175	90	110.57	12.78	15.35	14.63	13.71	13.62	13.91
38	36.1	40	13.1	1325	100	110.57	11.66	14.08	13.26	12.08	12.04	12.69
38	36.1	40	13.1	1572	120	110.57		12.48	11.47	10.11	10.21	10.51
38	36.1	40	13.1	1834	140	110.57		10.00	9.41	8.15	8.39	8.58
38	36.1	40	13.1	2096	160	110.57	--	8.01	7.48	6.61	6.92	6.65
38	36.1	40	13.1	2358	180	110.57		6.48	5.77	5.43	5.75	5.25
38	36.1	40	13.1	2620	200	110.57		5.32	4.32	4.52	4.82	4.25

Table 1: Experimental, analytical and numerical results.

* experimental results of bars under compression;

^{1,2,3,4} Resistances based on standards: ABNT NBR 16239:2013 [26]; ANSI/AISC 360-16 [27]; Eurocode 3 Part 1.4 [28], and CSA-S16 [29].

In the analysis of the results presented in Tab. 1, the first fact noted is the approximately constant distance between the compressive strength curves of the numerical and analytical front models, specifically in the region of higher slenderness ratios. The difference in resistance load between the curves, taking the normative values ABNT NBR 16239:2013 [26] and ABNT NBR 8800:2008 [31] as a reference, varies between the limits of 16 and 25%. Since the main dimensions and their boundary conditions were applied in an equivalent way in the two proposed approaches, such a difference is attributed to the consideration of residual stresses in the normative formulations and their respective absence in the numerical models. When evaluating the results collected for bars with slenderness ratios lower than 80, it is noted that the characteristic strength of the profiles determined by the criteria of the ABNT NBR 8800:2008 [31] code exceeds that predicted by the numerical tests. In their simulations, the local failure of the flattened ends is demonstrated on the numerical front as a limiting factor to the axial compressive strength load of the bars contained in this range of the spectrum of slenderness ratios. This fact can be graphically recognized by the horizontal portion of the modified P_{ult} – Numerical analysis curve in Fig. 16. The resistance load difference between the numerical and analytical curves reaches percentages of up to 24%, in relation to the reference values predicted by the code. In this way, the limitation of the normative analytical formulations to deal with the case is required, by partial adjustments in the process of designing short and medium slender bars or a broad reformulation of the equations that involves the whole spectrum of slenderness ratios.

CONCLUSIONS

With the objective of deepening the understanding of the phenomena of global and local instabilities of three-dimensional trusses constituted by end-flattened steel bars and typical bolted connections, this study demonstrated, through a series of numerical models the structural behavior of these elements when individually subjected to compressive loads.

From the development of numerical models with the aid of the Abaqus® software, subdivided into a couple of simulation phases with prototypes of slenderness ratios (λ) ranging from 20 to 200, two main forms of failure of the bars with flattened ends were observed, namely: the global buckling, characterized by the lateral displacement along the length of the axially compressed profiles; and the local instabilities of the transition zones of cross-sections of the models tested. The first of these was noted in the slenderest prototypes, being the ultimate resistance load of the profiles a function of this same property. Additionally, the short and medium slender models presented the second form of failure listed and converged approximately on a single resistance load value, so that local failure due to excessive deformation of the ends of the bars constituted a limiting threshold of characteristic resistance load. It is noteworthy that, for the prototypes with slenderness



ratios between 100 and 140, a transition between the aforementioned failure modes was observed, in which both were combined in variable proportions upon reaching the axial compressive strength of the modeled bars.

Referring to the bars with slenderness ratios from 100 to 200, the analysis by the modified Riks method was complemented by the previously processed modal analysis to enable the manifestation of global buckling for those models that presented susceptibility to this phenomenon. With the results collected for the model with such slenderness, its compatibility with the model referring to the first phase of the numerical analysis is evidenced, in terms of the failure mode due to excessive deformation and collapse of the ends of the prototypes, as well as in terms of the magnitude itself of the ultimate compressive strength load presented by both. The product of the simulations with the slenderer models, when arranged in increasing order of slenderness ratios, indicates a progressive reduction in the ultimate resistance load of the prototypes. A characteristic aspect of this set of simulations is the failure mode of the specimens, in which global buckling was predominant over local instabilities at the flattened ends of the bars.

In order to derive equations that can analytically and statistically represent the structural behavior of the end-flattened steel bars, parametric experimental tests should be carried out. A range of geometric and mechanical properties of the profiles should be tested, such as their diameter-to-thickness ratios and the yield stress of the steel. In any case, regarding the criteria to be used in the design of three-dimensional truss bars, the consideration of eccentricities in the connections of the profiles, especially in their diagonal elements, whose longitudinal axes in general have a distance not negligible to the lines of action of the requesting normal loads, is of notorious importance. Such normal load eccentricities translate into a state of flexure associated with tension or compression of the profiles, which reduces their resistance compared to simple situations of axial load.

Finally, for the bar models with axial compressive strength determined by the normative criteria of the Brazilian code ABNT NBR 8800:2008 [31], an approximately constant and non-negligible difference in strength was observed between the numerical and analytical approaches of the profiles with the highest slenderness ratios of the spectrum under study. This difference was attributed to the consideration of residual stresses in the normative formulations, which in turn predict a lower resistance to this set of structural elements. As for bars with slenderness ratios lower than 80, the resistance loads established by the reference code exceeded those of numerical tests by up to 24%. Due to the fact that the flattened ends of the bars limit the resistance value of the short and medium slender profiles and change the moments of inertia of these regions in the profiles in general, adjustments or integral reformulation of the code criteria for dimensioning linear elements submitted to axial compression loading for consideration of the present case are required.

REFERENCES

- [1] Bezerra, L. M., Freitas, C. A. S., Matias, W. T., Nagato, Y. (2009). Increasing load capacity of steel space trusses with end-flattened connections, *J. Const. Steel Res.*, 65, pp. 2197-2206. DOI: 10.1016/j.jcsr.2009.06.011.
- [2] Silva, W.V., Silva, R., Bezerra, L.M., Freitas, C.A.S., Bonilla, J. (2020). Experimental Analysis of Space Trusses Using Spacers of Concrete with Steel Fiber and Sisal Fiber. *Materials* 13, 2305. DOI: 10.3390/ma13102305.
- [3] Silva, W. V., Bezerra, L. M., Freitas, C. S., Bonilla, J., Silva, R. (2021). Use of Natural Fiber and Recyclable Materials for Spacers in Typical Space Truss Connections, *J. Struct. Eng.*, 147(8). DOI: 10.1061/(ASCE)ST.1943-541X.0003018.
- [4] Freitas, C. A. S., Silva, W. V., Bezerra, L. M., Júnior, F. F. S. M., Neto, V. C. P., Ribeiro, B. A. T. (2019). Experimental analysis of space trusses with typical connections reinforced with steel and sisal-resin spacers, *Adv. Steel Const.*, 15(4), pp. 398-405. DOI: 10.18057/IJASC.2019.15.4.10.
- [5] Freitas, C. A. S., Bezerra, L. M., Araújo, R. M., Sousa, E. C., Araújo, G. M., Bezerra, E. A. (2017). New experimental results of the research on reinforced node in space truss, *Adv. Steel Const.*, 13(1), pp. 30-44. DOI: 10.18057/IJASC.2017.13.1.2.
- [6] Yang, Y.-B., Yang, C.-T., Chang, T.-P. and Chang, P.-K. (1997). Effects of member buckling and yielding on ultimate strengths of space trusses. *Engineering Structures*, 19(2), pp. 179–191. DOI: 10.1016/S0141-0296(96)00032-6.
- [7] Martin, R. and Delatte, N. J. (2001). Another look at Hartford Civic Center Coliseum collapse, *J. Perform. Constr. Facil.*, 15(1), 31–36.
- [8] Bardi, F. C. and Kyriakides, S. (2006). Plastic buckling of circular tubes under axial compression—part I: Experiments. *International Journal of Mechanical Sciences*, 48(8), 830–841. DOI: 10.1016/j.ijmecsci.2006.03.005.
- [9] Caglayan, O., and Yuksel, E. (2008). Experimental and finite element investigations on the collapse of a Mero space truss roof structure – A case study. *Engineering Failure Analysis*, 15(5), pp. 458–470. DOI: 10.1016/j.engfailanal.2007.05.005.



- [10] Brencich, A. (2010). Collapse of an industrial steel shed: A case study for basic errors in computational structural engineering and control procedures. *Engineering Failure Analysis*, 17(1), pp. 213–225. DOI: 10.1016/j.engfailanal.2009.06.015.
- [11] Augenti, N. and Parisi, F. (2013). Buckling Analysis of a Long-Span Roof Structure Collapsed during Construction. *Journal of Performance of Constructed Facilities*, 27(1), pp. 77–88. DOI: 10.1061/(ASCE)CF.1943-5509.0000302.
- [12] Piroglu, F. and Ozakgul, K. (2016). Partial collapses experienced for a steel space truss roof structure induced by ice ponds. *Engineering Failure Analysis*, 60, pp. 155–165. DOI: 10.1016/j.engfailanal.2015.11.039.
- [13] Pieraccini, L., Palermo, M., Trombetti, T. and Baroni, F. (2017). The role of ductility in the collapse of a long-span steel roof in North Italy. *Engineering Failure Analysis*, 82, pp. 243–265. DOI: 10.1016/j.engfailanal.2017.07.012.
- [14] Klakurková, L., Horynová, M., Juliš, M., Gejdoš, P., Skalka, P., Remešová, M. and Čelko, L. (2017). Failure analysis of massively failed compressed air cartridge. *Engineering Failure Analysis*, 82, pp. 776–782. DOI: 10.1016/j.engfailanal.2017.07.016.
- [15] Wang, H., Wu, Q., Qian, H., Han, K. and Fan, F. (2019). Buckling behavior of a circular steel tube with a bolt–ball joint under installation eccentricity. *Engineering Structures*, 197, 109407. DOI: 10.1016/j.engstruct.2019.109407.
- [16] Tüfekci, M., Tüfekci, E., Dikicioğlu, A. (2020). Numerical Investigation of the Collapse of a Steel Truss Roof and a Probable Reason of Failure. *Appl. Sci.* 10, 7769. DOI: 10.3390/app10217769.
- [17] Alegre, V., Ródenas, V. and Villalba, S. (2012). Colapso de la cubierta metálica de un polideportivo; patologías singulares y recurrentes. *Revista ALCONPAT*, 2(1), pp. 37 - 45. DOI: 10.21041/ra.v2i1.25.
- [18] Terwel, K. (2021) Contributing human and organizational factors to the collapse of the FC Twente stadium roof Structural. IABSE Congress Ghent 2021, pp. 1565-1571. DOI: 10.2749/ghent.2021.1565.
- [19] Huibert B., Barbara R., Henco B. (2021) Collapse of the roof of a football stadium. IABSE Congress Ghent 2021, pp. 1055-1062. DOI: 10.2749/222137814814067257.
- [20] Michael, A. O., and Razak, A. R. (2013). The study of claims arising from building collapses: case studies from Malaysia, Nigeria, Singapore and Thailand. *Civil and Environmental Research*, 3(11), 113-129.
- [21] Gul, F. A. and Ali, C. M. (2016). Sultan Mizan Zainal Abidin Stadium Roof Collapse, Kuala Terengganu, Malaysia (Lack of Safety Issues). *EPH-International Journal of Mathematics and Statistics*, 2, pp. 14-23.
- [22] Dundu, M. (2014). Effect of flattening circular hollow sections in truss and dome structures. *Thin-Walled Structures*, 80, pp. 57–65. DOI: 10.1016/j.tws.2014.02.023.
- [23] Silva, W. V. (2020). Estudo experimental, estático e dinâmico, analítico e numérico de estruturas tridimensionais em aço com correções na ligação típica estampada. Doctoral thesis, University of Brasilia, Brazil. <https://repositorio.unb.br/handle/10482/41527> (Accessed on 23 August 2022).
- [24] Inc., A. ABAQUS/Explicit, (2016); Dassault Systèmes Simulia Corp: Johnston, RI, USA.
- [25] ABAQUS (2016). Theory Manual, User Manual and Example Manual Version 6.14., Dassault Systemes Simulia Corp.
- [26] ASSOCIAÇÃO BRASILEIRA DE NORMAS TÉCNICAS. NBR 16239 – Projetos de Estrutura de Aço e de Estruturas Mistas de Aço e Concreto de Edificações com Perfis Tubulares, Rio de Janeiro, (2013).
- [27] ANSI/AISC 360-16. Specification for Structural Steel Buildings. Chicago, (2016).
- [28] EUROCODE 3: Design of steel structure. Part 1-1: General rules and rules for buildings. Brussels, (2003).
- [29] CAN/CSA-S16-09, Limit States Design of Steel Structures, Canadian Standard Association, Rexdale, (2009).
- [30] Mazon, A. A., Sarmanho, A., Nunes, G., Roquete, L., Neiva, L. H. and Souza, F. (2018). Numerical analysis of truss systems with stiffened flattened end-bars. *Latin American Journal of Solids and Structures*, 15(3). DOI: 10.1590/1679-78254119.
- [31] ASSOCIAÇÃO BRASILEIRA DE NORMAS TÉCNICAS. NBR 8800: Projeto de estrutura de aço e estruturas mistas de aço e concreto de edifícios. Rio de Janeiro, (2008).
- [32] Gardner, L., Talja, A. and Baddoo, N. R. (2006). Structural design of high-strength austenitic stainless steel. *Thin-Walled Structures*, 44(5), pp. 517–528. DOI: 10.1016/j.tws.2006.04.014.
- [33] Rondal, J. and Maquoi, R. (1981). Closure to Single Equation for SSRC Column-Strength Curves. *Journal of the Structural Division* pp. 247-250. DOI: 10.1061/JSDEAG.0005738.
- [34] Hansen, T. (2006). Theory of plasticity for steel structures – Solutions for fillet welds, plate girders and thin plates. PhD thesis, Technical University of Denmark, Birch and Krogboe A/S Consultants and Planners, Denmark.
- [35] Souza, A. S. C., Gonçalves, R. M., Nardin, S., Calado, L. (2008). A strategy of numerical analysis of space truss connections with stamped bar ends, *Int. J. Space Struct.*, 23(3), pp. 143-152. DOI: 10.1260/0266351087862610.
- [36] Souza, A. S. C., Gonçalves, R. M., Maiola, C. H., Malite, M. (2003). Theoretical analysis of the structural performance of space trusses commonly used in Brazil, *Int. J. Space Struct.*, 18(3), pp. 167-179. DOI: 10.1260/02663510332243.